Mini Twist: A Study of Long-Range Linear Drive by String Twisting

James J. Guzek
e-mail: jjg45@cornell.edu

Conrad Petersen
e-mail: ctp32@cornell.edu

Mechanical and Aerospace Engineering,
Cornell University,
Ithaca, NY 14853

Stephane Constantin
Electrical and Computer Engineering,
Cornell University,
Ithaca, NY 14853
e-mail: sc445@cornell.edu

Hod Lipson
Electrical and Computer Engineering,
Computing and Information Science,
Cornell University,
Ithaca, NY 14853
e-mail: hod.lipson@cornell.edu

Published methods of linear actuation via string transmission are discussed. A novel twisting string actuator design named Mini Twist is introduced. The design and components of the Mini Twist are thoroughly explained, and a theoretical model for its transmission method is discussed. The experimental set-up is defined. Experimental data regarding the relationship between string diameter, string tension, strand count, and strand type is presented, and analysis of the data is provided. The features of the actuator and the validity of the theoretical model are summarized.
[DOI: 10.1115/1.4005331]

Keywords: linear actuator, string twisting actuation, optical encoder, strain gauge applications, ABS plastic printing

1 Introduction

Advances in the robotics field over the past few years have created a need for compact and precision linear actuation devices to power these systems. As a result, a variety of actuators have been created in order to supply this need. A common transmission method employed by many of these devices involves the combination of one or more strings actuated by a motor-powered rotor. In recent literature, a variety of string/rotor combinations have been presented. Many of these devices use a string spooling design similar to a winch. Spooling actuators have been found to be a simple and effective method of applying tension, torque, or displacement in robotic applications [1–9].

Other researchers have found the method of linear actuation via string twisting to be a preferred and more precise design. Twist actuation is a mechanical process in which a group of parallel fiber strands of the same length are helically wound in order to decrease the overall axial length of the strand group. In this paper, an assembly of two or more strands is collectively referred to as a *string*. Typically, one end of a string is tied to a point to be moved and the other end to a driving mechanism. As the number of rotations applied to a strand group increases, the helix becomes more tightly wound and the axial string length decreases.

Although patents regarding this design date back to 1933 [10], the theoretical modeling of twist actuation appears to have been first investigated in the literature by Costello and his colleagues (1977) [11], who determined the mathematical relationship between the number of rotations, torsional stiffness, and axial load in a group of strands. In his 1997 publication, Costello built upon this model by analyzing the strand geometry in order to establish theoretical equations for the axial strain, rotational strain, and internal stresses inherent in individual strands [12]. More current publications present the fabrication and experimental testing of motor-driven twist actuation devices. Designs such as Shoham's twisting wire actuator have demonstrated extraordinary precision down to two microns [13]. Several robotic applications of twist actuators, such as a multi-actuator prosthetic hand, have also been described in recent engineering papers [14–16].

The objectives of this paper are to present the design of a twist actuator named Mini Twist, to derive a theoretical model to characterize the twisting strands, and to determine the model's validity through experimental testing. A practical application of the actuator in a modular robot named the Cube is also briefly discussed. Individual Cube modules are capable of preprogrammed actuation and can be easily assembled side-by-side to create a robot of greater complexity.

2 Methods

2.1 Methods—Mechanical Design. We present a twist actuator named Mini Twist that is compact, lightweight, and wirelessly controlled. Moreover, it is multifunctional. The actuator is intended for precision robotic applications and is capable of measuring the number and direction of driveshaft rotations, and the magnitude of string tension.

A small DC-powered motor, the Solarbotics GM12a 100:1 Mini Metal Gear Motor was chosen as its driving mechanism for its size, output, and reasonable cost. It is quite compact (2.8 cm × 0.99 cm × 1.19 cm), has minimal mass (8.22 g), and is powered by 48 mA of current.

A case for the motor was designed in Solidworks™ and fabricated with a 3D ABS-plastic printer. The case has three main components: the body, faceplate, and nozzle, shown from left to right in Fig. 1(*b*). When assembled, the motor sits tightly within the hollow of the casing's body. The nozzle fits snuggly onto the motor's driveshaft by matching the driveshaft's notched geometry. The nozzle also fits through the central hole in the faceplate, which tightly reinforces it to the motor. Its flared base sits loosely in the cylindrical notch in the faceplate, allowing for nozzle rotation. The case also features clasps on both sides to hold two 230 mA DC batteries for powering the device.

The components are joined with screws and threaded thermoplastic insert fasteners. The fasteners are manually inserted into the case body with a soldering iron, and 2–56 screws hold the faceplate to the body through the three holes in the corners of the faceplate. For application, the case is anchored to a location by a wire loop inserted through the brackets on the rear of the vertical plate. One or more strands to be twisted are looped through the hole in the nozzle tip. Nylon strand was found to be best suited for this role due to its durability and resistance to stretch.

The Mini Twist employs an optical encoder to measure rotation and a strain gauge to determine string tension. The E4P OEM Miniature Optical Encoder screws into the faceplate and fits around the nozzle. Its resolution is measured in 360° rotation increments. The strain gauge (Omega SGD-1.5/120-LY11) is glued to the inside of the vertical plate at the rear of the casing body. As the string tension increases by progressive twisting, the vertical plate increasingly bends backwards, stretching the strain gauge. Using a load cell, the strain gauge can be calibrated by

Contributed by the Mechanisms and Robotics Committee of ASME for publication in the Journal of Mechanisms and Robotics. Manuscript received February 24, 2010; final manuscript received September 22, 2011; published online February 3, 2012. Assoc. Editor: Jian S. Dai.

 Copyright © 2012 by ASME

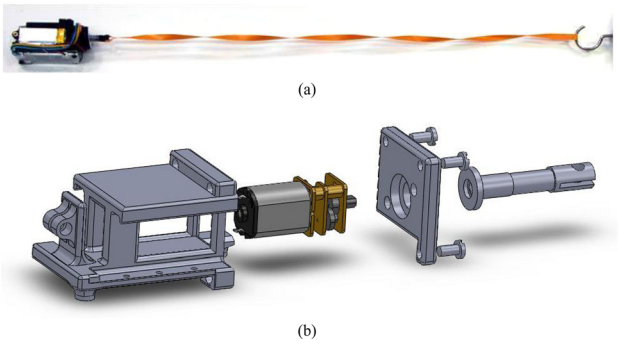


Fig. 1 Linear twist actuator: (*a*) fully assembled twist actuator; (*b*) exploded diagram of twist actuator case

correlating the magnitude of gauge's resistance readings with force measurements.

A printed circuit board (PCB) screws into the bottom of the case, and is hardwired to the motor, optical encoder, and strain gauge. It has a Radiotronix Wi232FHSS-25 R module for wireless communication and control by a desktop computer. The PCB serves two important functions via this wireless link: it receives motor twist/stop/untwist commands from the computer and continuously conveys strain gauge and optical encoder measurements to an electronic record on the computer. To protect against damage, an acrylic sheet cut to match the PCB's geometry covers the board (Fig. 2(*c*)).

The desktop computer has a JAVASCRIPT control program and a wireless communication board and serves as the controlling/recording device for the actuator. The controller circuit on the communication link is an ATMEGA32L microcontroller. It conveys commands to the motor via an external H-Bridge circuit. The strain gauge signal is read with an incorporated analog to digital (ADC) converter on the PCB, and the optical encoder digital signals are read by triggering an external interrupt. Please refer to the appendix for an electrical schematic of the circuit.

If several actuators are to be used simultaneously, the control program can communicate with them to collectively operate in a synchronized manner. In addition, each actuator can be individually controlled by a user addressing mode that distinguishes the actuator by its MAC (Media Access Control) Address. For

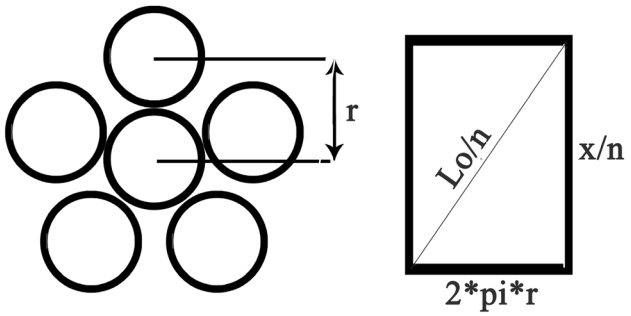


Fig. 3 Visual representations of geometric aspects of a twisted cord: (*a*) cross section of a bundle of strands; (*b*) flattened representation of a single helical twist

intended robotic applications, sequences of preprogrammed commands for numerous actuators can also be run by the program.

2.2 Methods—Performance Modeling. In this section, a static theoretical model that characterizes the behavior of helically twisted strands will be derived. The model is based on the geometry and properties of a twisted string and the Pythagorean Theorem. Subsequently, the elastic deformation and compression of a string are considered, and their influence on the model is evaluated.

2.2.1 Helical Geometric Model. When two or more strands are twisted, each strand follows a helical path about the rotational axis at the center of strand bundle. As the number of strands (strand count) in a string increases, the outermost strands will have the greatest influence on the length change of the string. In the cross section of a string, the distance from the rotational axis to the core of an outermost strand is represented by the variable *r*, which is depicted in Fig. 3(*a*).

The string is most simply visualized as a cylinder, with the outer strands following helical paths along the outer edge of the cylinder. If this cylinder were viewed from the side two-dimensionally, it would appear to be rectangular. Figure 3(*b*) shows this representation for a single 360° twist. The diagonal bold line represents the path of an outer strand in a vertically

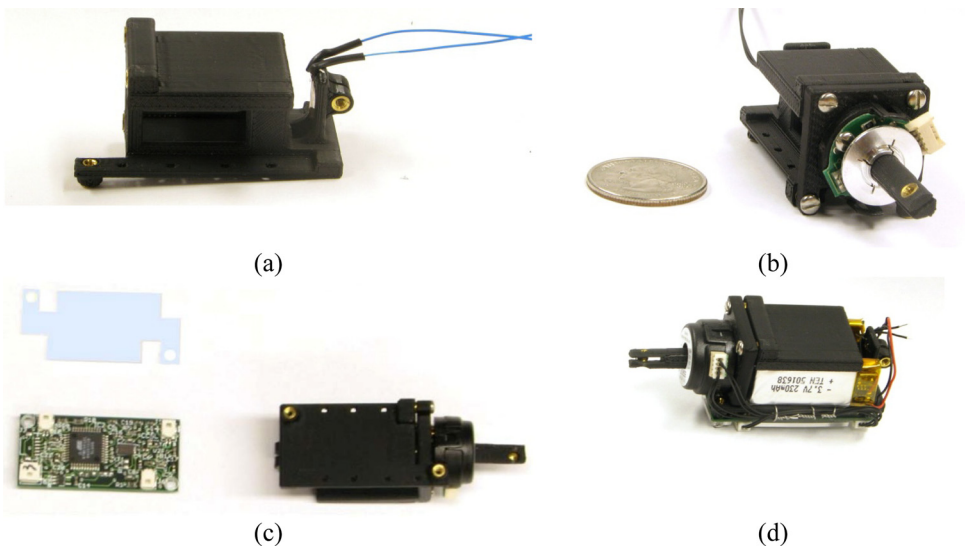


Fig. 2 Assembly of twist actuator components: (*a*) actuator casing body. Note the strain gauge plate in the back. (*b*) Assembled actuator casing, with optical encoder on nozzle. Pictured with quarter. (*c*) PCB, blue PCB cover, and bottom of actuator showing screw holes. (*d*) Fully assembled actuator, with optical encoder cap. Twist ties hold loose wires tightly to the actuator through holes in the body, located below the battery compartment.

standing cylinder, and the horizontal bold lines represent the cylinder circumference at the ends of the cylinder. This representation will be used to determine the relationship between the path length of the outer strand L_0, the radius of the cylinder r, length of the cylinder x, and the number of 360° twists n.

From Pythagorean Theorem [17]

$$\left(\frac{x}{n}\right)^2 + (2\pi rn)^2 = \left(\frac{L_O}{n}\right)^2 \rightarrow x = \sqrt{L_O^2 - (2\pi rn)^2} \tag{1}$$

String tension can skew the accuracy of this model. This deviation is due to two factors: strand stretching and strand compression. Stretching occurs via elastic deformation due to the material properties of the strand, and compression of inner strands results from the outer helical strands applying radially directed force. This compression can cause a decrease in overall string diameter. These factors have the potential to drastically affect the accuracy of this model and will be examined further in the following subsections.

2.2.2 Model Consideration #1—Strand Elongation Due to Elastic Deformation. In order to determine the effect of strands' elastic stretching due to tension upon the overall string length, the linear elastic relationship of an individual strand is considered. In this model, the cross sectional area of one strand is represented by A, the strand's Young's modulus by E, the applied load via tension by $P_{\|}$, the change in strand length by δ, and the final strand length by L_x.

Starting with the elastic relationship [18]

$$\delta = \frac{P_{\|} L_O}{AE} \tag{2}$$

$$P_{\|} = \frac{PL_x}{x} \tag{3}$$

$$\delta = \frac{PL_O L_x}{AE} \tag{4}$$

$$L_x = L_O + \left(\frac{PL_O L_x}{AEx}\right) \tag{5}$$

$$L_x = \frac{L_O}{1 - \dfrac{PL_O}{AEx}} \tag{6}$$

Equation (6) can be used to evaluate the strand length change due to stretching. The dimensions and material properties of the strand type used in experimental testing are as follows: $L_0 = 0.4064$ m, $r = 9.525 \times 10^{-4}$ m, $A = 2.8502 \times 10^{-6}$ m^2, $E = 2.0684 \times 10^{11}$ Pa, $G = 7.722 \times 10^{10}$ Pa. When a typical tension of 2.223 N is applied to the strand, the length of the strand increases to $L_x = 0.4064015324$ m. This corresponds to a negligible increase of 0.00038% in strand length. When compared to the significant length changes due to string twisting, the effects of elastic deformation can be ignored.

2.2.3 Model Consideration #2—Strand Compression Due to String Tension. The tension created in a twisting string can also cause a decrease in string diameter, due to compression caused by outer strands. This phenomenon also needs to be considered in the helical model. Equation (7) shows the relationship between strand diameter d_s, the change in strand diameter δ_d, and the modulus of rigidity G. The change in diameter is based on the relationship between orthogonal strains through Poisson's ratio [18]

$$\delta_d = \delta_s \left(\frac{L_x}{L_O} - 1\right)\left(1 - \frac{E}{2G}\right) \tag{7}$$

Equation (7) can be substituted into Eq. (1) to evaluate the effect of compression upon overall string length

$$x = \sqrt{L_x^2 - \left(\pi nd\left(1 + \left(\frac{L_x}{L_O} - 1\right)\left(\left(1 - \frac{E}{2G}\right)\right)\right)\right)^2} \tag{8}$$

Using the same values as in the above consideration, there is a change of 0.023% in strand diameter or 0.058% in effective string length. Once again, this consideration is found to be insignificant under the test conditions used.

2.2.4 Model Consideration #3—Strand Packing. The geometry of the string cross-section must also be examined in order to accurately implement the model presented earlier. The most significant change that can occur in this model is a change in the value for d, the mean diameter of the string helix. This value is highly dependent on the way in which the strands pack together when twisted. Although this value should be consistent over repeated tests, it is not easily determined for larger numbers of strands.

The packing configurations shown in Fig. 4 were considered when modeling the effective length function for different numbers of strands. Although some configurations are more likely to occur than others, it is very difficult to predict exactly how the strands will be configured within the helix. Configurations were chosen based on their theoretical viability as well as their correlation with the experimental data.

2.2.5 Spring Constant Due to Strand Packing. As a string becomes highly twisted, it develops the potential to act like a spring. Therefore, the effect of twisting upon a string's spring constant k must also be considered. In general, the relationship between the spring constant and the number of twists in the string is inversely proportional. This has resulted in two common methods for determining axial deflection via $\boldsymbol{k}$ in a twisted medium: the open-coiled helical spring model and the close-coiled helical spring model.

The deflection equation of the open-coiled model is based upon the degree of string twisting. Take, for example, a multistrand string with no twists. As the string begins to twist, the axial string length shortens and the strands become increasingly helically coiled. Concurrently, an angle α is formed between the cross-sectional plane of the string and the direction of the helix strands. This angle decreases from 90 deg toward 0 deg as the number of twists increases.

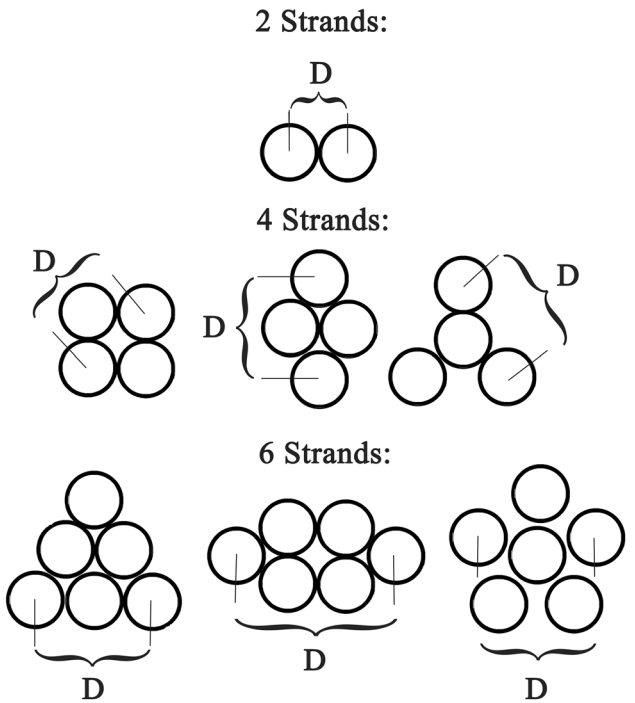


Fig. 4 Strand packing diagrams for various numbers of strings

In order to incorporate the effect of string twisting into the deflection equation, α is included as the expression $\sec(\alpha)$ in the open-coiled axial deflection equation. As α progresses from 90 deg toward 0 deg, the value of $\sec(\alpha)$ decreases from infinity toward 1. On the other hand, the close-coiled model does not take the extent of twisting into account. Rather, it considers the strands to be so highly twisted that the angle α is assumed to be 0 deg. As a result, the close-coiled deflection equation below is independent of α [15]. In Eq. (9), D is the mean diameter of the helix, d_s is the diameter of an individual strand, and n is number of 360 deg twists.

$$\delta = \frac{8PD^3n}{Gd_s^4} \tag{9}$$

Using the same values as in the above sections, the length change based on the closed-coil model is calculated. For two, four, and six strand bundles, the values inputted for n are the maximum number of twists measured during experimental testing. The length changes for these bundles are calculated to be 8.489×10^{-6} m, 3.536×10^{-5} m, and 3.881×10^{-5} m, respectively. Again, the deflections caused by a string's spring constant are significantly less than 1% in all three scenarios. Therefore, this consideration can also be disregarded in the model.

Despite the fact that the open-coiled model may more accurately determine the deflection of a twisted string, the close-coiled model was chosen for this consideration. Several factors, including strand packing and string tension, affect the value of the helical angle. Since these influences may fluctuate largely in different scenarios, the close-coiled model was evaluated since it is independent of these variables and, therefore, more predictable and suitable for general applications.

2.2.6 Final Model After Considerations. After careful consideration of the many different phenomena occurring within the twisting medium, the geometric aspect of the helix seems to be the only significant factor. Thus, the effective length of a twisted string as a function of the number of turns applied is modeled by our original equation

$$x = \sqrt{L_O^2 - (2\pi rn)^2} \tag{10}$$

3 Results

Experiments were performed to determine the effects of string tension, strand count, strand diameter, and strand type upon the length of a twisting string. All trials were performed in three sequential loops from zero twists to a point where the string began to exhibit nonlinear bunching. The experimental set-up hung the Mini Twist vertically, allowing the string to dangle freely. The strand types used in Fig. 6(*d*) are a ribbon which is 0.254 cm wide, 2 nylon strands which are 0.1067 cm in diameter each, and 6 metal wire strands which have a diameter of 0.0305 cm each. A clip was attached to the end of the string to prevent it from spinning. To gauge the accuracy of the theoretical model, experimental results were plotted with theoretical results obtained from the model.

4 Discussion

From the results above, a number of deductions can be made about the change in string length when different variables are applied. Figure 5(*a*) shows the relationship between string tension and string length. The actuator was hung vertically, and tension

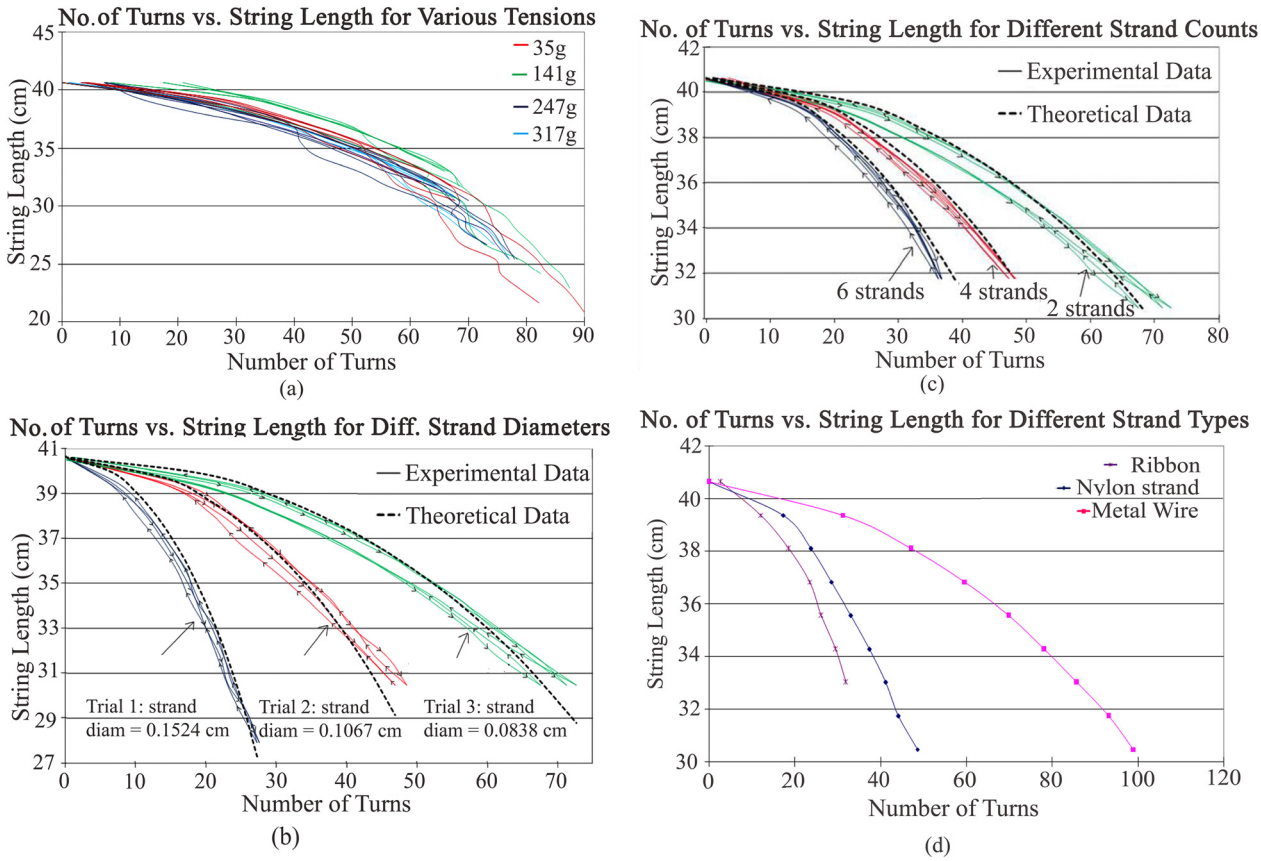


Fig. 5 Plots of actuator data: (*a*) graph of number of motor turns versus string length for a variety of tensions, for a strand of 0.0838 cm diameter. (*b*) Graph of length of string versus number of turns of motor for strings with different numbers of strands, but fixed tension for string of 0.1067 cm diameter. (*c*) Graph of string length versus number of turns for strings with different strand diameter, but fixed strand number and tension. (*d*) Graph of length of string versus number of turns of motor for different strand types.

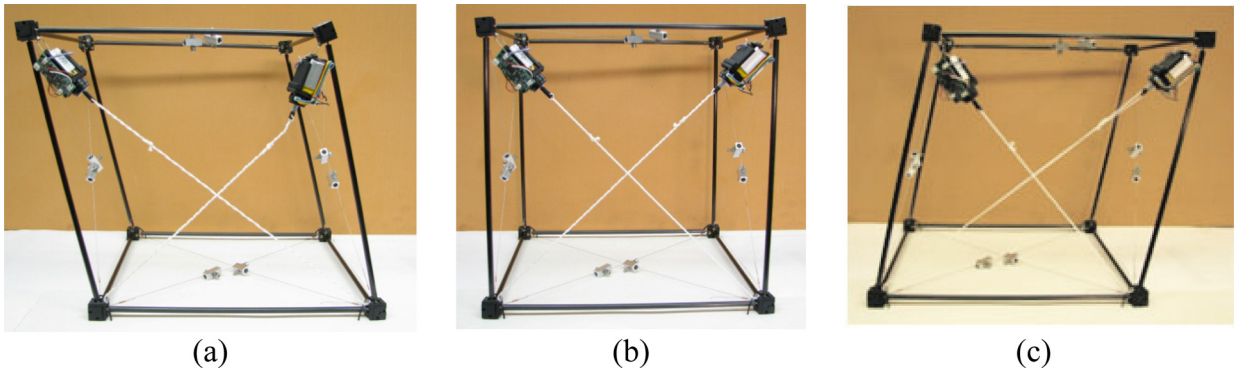


Fig. 6 Cube robot at different angles: (*a*) cube leaning left; (*b*) cube upright, with both strings of equal length; (*c*) cube leaning right

was applied by attaching a mass to the end of the actuator string. The strand count was two, and the masses varied between 35 and 317 g. The results for all of the trials were quite similar; they showed a close parabolic trend as the string shortened via twisting from a length of 0.4064 m to a minimum length of 0.2540 m. However, these trials did not display any trend of increasing length with an increase in tension. As a result, elasticity cannot be attributed to the string at any degree of twisting. This conclusion is supported by the theoretical model, since the effect of string elasticity was determined to change overall string length by less than 1%.

Figure 5(*b*) shows the relationship between strand diameter and the change in string length. The experimental results show that string length changes more rapidly as the strand diameter is increased. For each of the three trials, the theoretical model posed is a quite accurate prediction of length change; the experimental length distribution decreases more quickly than the theoretical data, but they differ only by approximately two motor turns for each of the trials. This discrepancy may be a result of a slight difference between the reported and actual strand diameters, or an anomaly in strand packing.

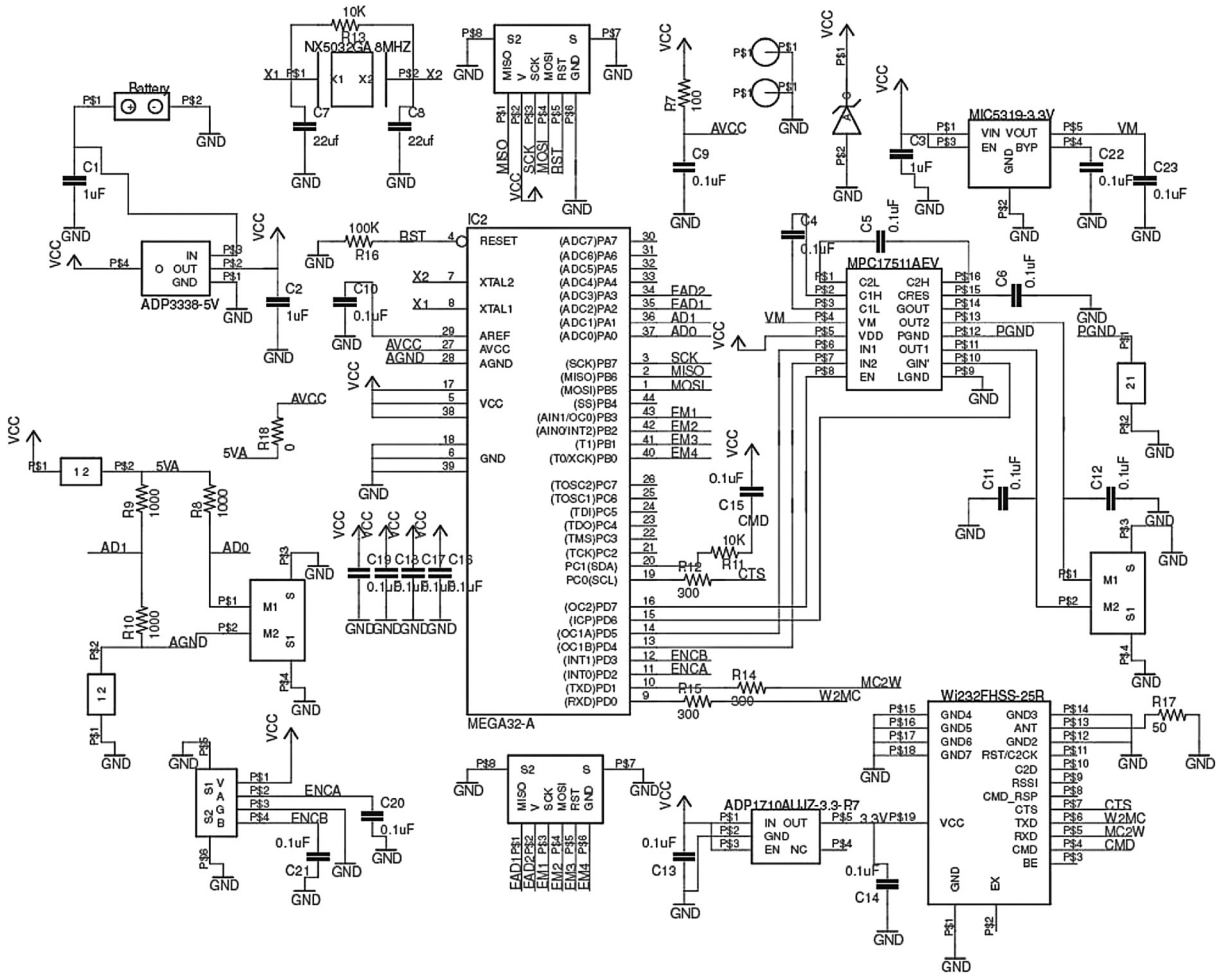


Fig. 7 Electrical schematic for actuator circuit board

Figure 5(*c*) is a plot displaying the relationship between strand count and the change in string length. The data shows that string length changes more rapidly as the number of strands is increased. In addition, the graph shows that results are repeatable over a sequence of tests, since the three tests recorded for each trial follow the same length distribution. Therefore, it can be deduced that the string undergoes no marked plastic deformation from repeated use. Also, experimental results and the theoretical model are quite similar for each of the trials. These results support the accuracy of the strand packing concept and Eq. (10).

Different string materials were tested to determine an optimal fiber to be used for the twist actuator. Figure 5(*d*) shows length distribution results for trials using ribbon, aluminum wire, and polyester string. Each of the materials has very different distributions, and therefore can possibly be used in different applications. However, it was determined that string is the most reliable material for use with the actuator. Not only does it resist any plastic deformation after repeated use, but it also is the most durable of the materials tested. On the other hand, the ribbon starts to exhibit bunching and other uncharacteristic winding below the effective length of 0.33 m, and the wire breaks after repeated testing.

5 Conclusion

The Mini Twist has a number of desirable features for robotic applications. It is constructed of cost-effective components and has a quick and simple assembly process. For its miniature size, it also exhibits a variety of functions: an optical encoder to measure motor turns, a strain gauge to measure string tension, and a circuit board to receive commands wirelessly and to convey encoder and strain gauge data to a computer. As a result, it is suitable for a wide variety of applications.

Experimental results show that the string length tends to show a parabolic distribution regardless of changes in variables or string material. The data shows a general trend of a more rapid decrease in string length with increase in string diameter and strand number. However, string tension appears to have no effect on this distribution. Moreover, the theoretical model proposed for string length distribution is quite accurate, showing minimal discrepancy from experimental data.

6 Applications

One application is the Cube, a cubical modular robot, which is extremely flexible, as a result of the ball-and-socket-joints connecting the carbon graphite rods at each corner of the structure. Twist actuators are connected across the diagonals of each face, for a total of 12 actuators per cube. The cube itself is able to adjust in many ways. The actuators can influence the cube to lean, transforming it from a square into a parallelogram. This displacement can be seen in Fig. 6. Also, the Cube can be actuated so that the vertical sides are twisted about the central axis of the cube. This robot can even exhibit motion by means of sequential rolling along adjacent faces.

The main feature of this design is the capability for multiple cubes to be assembled at any of their faces, giving a wide array of structural options for various applications. They can be united in multiple rows or layers of cubes without affecting functionality. There are a wide variety of applications for this design. Larger designs potentially include robotic arms, and larger robots with more complex forms of motion such as walking.

Acknowledgment

This work was supported in part by the U.S. National Science Foundation's (NSF) Office of Emerging Frontiers in Research and Innovation (EFRI), grant #0735953.

Appendix

Our circuit board (Fig. 7) is designed around the ATMEGA32L microcontroller from Atmel (Fig. 7). The microcontroller has on-board ADC converters, 8 bit and 16 bit timers, external interrupts, and UART serial communication. The microcontroller runs off an 8 MHz crystal, the NX5032GA-8MHZ-AT-W from *NDK*. A stable and accurate clock source was required to support the UART serial communication with the radio transceiver.

Most of the electronics, including the microcontroller, run from a 5 V supply. The 7.4 V from the batteries are regulated down to 5 V with the ADP3338AKCZ-5-R7 voltage regulator from *Analog Devices*. It can source up to 1 A of current which is plenty for our purpose. The radio transceiver runs at 3.3 V regulated by ADP1710AUJZ-3.3-R7 voltage regulator also from *Analog Devices*.

The H-Bridge IC MPC17511AEV from *Freescale Semiconductors* is used to drive the DC motor. It can output up to 1 A. The H-Bridge receives PWM signals from the 16 bit timer on-board the microcontroller.

The strain gauge used is the SGD-1.5/120-LY11 from *Omega*. It is a passive device that changes resistance when it deforms. The gauge is connected in a Quarter Bridge setup with 1 K resistors. The differential voltages from the bridge are fed to the AtoD converters on-board the microcontroller.

Signals from the E4P OEM optical encoder from *US Digital* are fed directly to the External Interrupt hardware of the microcontroller. This microcontroller interrupt has high-priority task of detecting a rising-edge signals from the optical encoder when it is rotating.

The radio transceiver used is the Wi232FHSS-25-R from *Radiotronix*. It has a simple UART communication interface with the microcontroller. The module allows user-addressing by MAC addresses, which facilitates the task of networking several of those modules. We module operates within a range of a few meters with only a 50 Ω resistor terminating the antenna line. For longer-range use, a standard antenna is required.

The circuit has the standard protection, bypass capacitors, high-frequency noise-suppressor beads to separate digital and power lines, and a protection diode.

References

[1] Kossowski, C., and Notash, L., 2002, "CAT4 (Cable Actuated Truss—4 Degrees of Freedom): A Novel 4 DOF Cable Actuated Parallel Manipulator," J. Rob. Syst., **19**(12), pp. 605–615.

[2] Cunningham, D., and Asada, H. H., 2009, "The Winch-Bot: A Cable-Suspended Underactuated Robot Utilizing Parametric Self-excitation," *Proceedings of the IEEE International Conference on Robotics and Automation*, L. Jingshan et al., eds., Kobe, Japan, pp. 1844–1850.

[3] Williams, R. L., and Gallina, P., 2003, "Translational Planar Cable-Direct-Driven Robot," J. Intell. Robotic Syst., **37**(1), pp. 69–96.

[4] Kawamura, S., Choe, W., Tanaka, S., and Pandian, S. R., 1995, "Development Of an Ultrahigh Speed Robot FALCON Using Wire Drive System," *Proceedings of the IEEE International Conference on Robotics and Automation*, K. Valavanis et al., eds., Nagoya, Japan, Vol. 1, pp. 215–220.

[5] Maeda, K., Tadokoro, S., Takamori, T., Hiller, M., and Verhoeven, R., 1999, "On Design of a Redundant Wire-Driven Parallel Robot WARP Manipulator," P. Luh et al., eds., *Proceedings of the IEEE International Conference on Robotics and Automation*, Detroit, Michigan, Vol. 2, pp. 895–900.

[6] Bostelman, R. V., Jacoff, A. S., Dagalakis, N. G., and Albus, J. S., 1996, "RCS-Based Robocrane Integration," *Proceedings of the International Conference on Intelligent Systems: A Semiotic Perspective*, Gaithersburg, MD.

[7] Williams II, R.L., Gallina, P., and Vadia, J., 2003, "Planar Translational Cable-Direct-Driven Robots," J. Rob. Syst., **20**(3), pp. 107–120.

[8] Fujiki, N., Mae, Y., Umetani, T., Arai, T., Takubo, T., and Inoue, K., 2005, "Limb-Mechanism Robot With Winch Mechanism," *Climbing and Walking Robots: Proceedings of the 7th International Conference, CLAWAR 2004*, Madrid, Spain, pp. 305–312.

[9] Apostolopoulos, D., and Bares, J., 1995, "Locomotion Configuration of a Robust Rappelling Robot," *Proceedings of the International Conference on Intelligent Robots and Systems*, Pittsburgh, Pennsylvania, pp. 280–284.

[10] Krummer, A., 1933, "System for Moving Bodies Towards and Away From Each Other," U.S. Patent No. 2,027,386.

[11] Costello, G. A., and Sinha, S. K., 1977, "Torsional Stiffness of Twisted Wire Cables," J. Engrg. Mech. Div., **103**(4), pp. 766–770.

[12] Costello, G. A., 1997, *Theory of Wire Rope*, 2nd ed., Springer-Verlag, London, England.

[13] Shoham, M., 2005, "Twisting Wire Actuator," ASME J. Mech. Des., **127**, pp. 441–445.

[14] Sonoda, T., and Godler, I., 2010, "Multi-Fingered Robotic Hand Employing Strings Transmission Name 'Twist Drive'," *Proceedings of the 2010 IEEE/RSJ International Conference on Intelligent Robots and Systems*, Taipei, Taiwan, pp. 2733–2738.
[15] Suzuki, M., and Ichikawa, A., 2005, "Toward Springy Robot Walk Using Strand-Muscle Actuators," M. A. Armada, and P. Gonzalez de Santos, eds., *Climbing and Walking Robots: Proceedings of the 7th International Conference CLAWAR 2004*, Madrid, Spain, pp. 479–486.
[16] Wurtz, T., May, C., Holz, B., Natale, C., Palli, G., and Melchiorri, C., 2010, "The Twisted String Actuation System: Modeling and Control," *Proceedings of the 2010 IEEE/ASME International Conference on Advanced Intelligent Mechatronics, AIM 2010*, Montreal, Canada, pp. 1215–1220.
[17] Jurgensen, R. C., Brown, R. G., and Jurgensen, J. W., 2000, *Geometry*, McDougal Littell Press, Chap. 4.
[18] Hearn, E. J., 1995, *Mechanics of Materials*, 2nd ed., Pergamon, Elsmford, New York.